Inhibitor Coordination Interactions in the Binuclear Manganese Cluster of Arginase[†,‡]

Evis Cama,[§,||] Stéphanie Pethe,[⊥] Jean-Luc Boucher,[⊥] Shoufa Han,[#,▽] Frances A. Emig,[@] David E. Ash,[@] Ronald E. Viola,[#] Daniel Mansuy,[⊥] and David W. Christianson*[,§]

Roy and Diana Vagelos Laboratories, Department of Chemistry, University of Pennsylvania, Philadelphia, Pennsylvania 19104-6323, UMR 8601 CNRS, Université Paris V, 45 Rue des Saints-Pères, 75270 Paris Cedex 06, France, Department of Chemistry, University of Toledo, Toledo, Ohio 43606, and Department of Biochemistry, Temple University School of Medicine, Philadelphia, Pennsylvania 19140

Received April 25, 2004; Revised Manuscript Received May 12, 2004

ABSTRACT: Arginase is a manganese metalloenzyme that catalyzes the hydrolysis of L-arginine to form L-ornithine and urea. The structure and stability of the binuclear manganese cluster are critical for catalytic activity as it activates the catalytic nucleophile, metal-bridging hydroxide ion, and stabilizes the tetrahedral intermediate and its flanking states. Here, we report X-ray structures of a series of inhibitors bound to the active site of arginase, and each inhibitor exploits a different mode of coordination with the $Mn^{2+}{}_2$ cluster. Specifically, we have studied the binding of fluoride ion (F^-; an uncompetitive inhibitor) and L-arginine, L-valine, dinor-N^{ω}-hydroxy-L-arginine, descarboxy-nor-N^{ω}-hydroxy-L-arginine, and dehydro-2(*S*)-amino-6-boronohexanoic acid. Some inhibitors, such as fluoride ion, dinor-N^{ω}-hydroxy-L-arginine, and dehydro-2(*S*)-amino-6-boronohexanoic acid, cause the net addition of one ligand to the $Mn^{2+}{}_2$ cluster. Other inhibitors, such as descarboxy-nor-N^{ω}-hydroxy-L-arginine, simply displace the metal-bridging hydroxide ion of the native enzyme and do not cause any net change in the metal coordination polyhedra. The highest affinity inhibitors displace the metal-bridging hydroxide ion (and sometimes occupy a $Mn^{2+}{}_A$ site found vacant in the native enzyme) and maintain a conserved array of hydrogen bonds with their α-amino and -carboxylate groups.

Arginase is a binuclear manganese metalloenzyme that catalyzes the hydrolysis of L-arginine to form L-ornithine and urea (*1*−*5*). Two isozymes exist in mammals: the hepatic arginase I and the extrahepatic arginase II. Arginase I catalyzes the final cytosolic step of the urea cycle in liver cells and is a 105 kDa homotrimer (*6*, *7*). Each 35 kDa monomer contains a binuclear manganese cluster that is required for catalytic activity, located at the bottom of a 15 Å deep active site cleft (*8*). In the native enzyme, a hydroxide ion symmetrically bridges the two manganese ions and donates a hydrogen bond to Asp-128, thus leaving one lone electron pair available for nucleophilic attack at the substrate (*8*). Arginase II functions primarily in L-arginine homeostasis in nonhepatic tissues (e.g., in regulating L-arginine bioavailability to nitric oxide synthase (*1*−*5*, *9*−*12*)). Human arginases I and II are related by 50% amino acid sequence identity, and residues important for metal coordination and substrate binding and catalysis are strictly conserved between the two isozymes.

The simplest inhibitor of arginase is the fluoride ion (*13*−*16*), which is an uncompetitive inhibitor with $K_i = 1.3$ mM (*13*). As such, the binding of substrate L-arginine is required to produce the form of the enzyme to which the F^- ion binds. Fluoride inhibition likely involves a novel coordination interaction with the binuclear manganese cluster, but kinetic analyses performed to date have not indicated the nature of this interaction. Other simple inhibitors of arginase include a number of inert amino acids (*17*), including branched hydrophobic amino acids such as L-valine ($K_i = 3.6$ mM) (*18*, *19*). It is proposed that inhibition arises from either the displacement of the metal-bridging hydroxide ion or the increase of the intermanganese separation, thus compromising the metal-activated hydroxide ion (*20*).

More complex amino acid inhibitors of arginase contain functionalized side chains (Table 1), such as N^{ω}-hydroxy-L-arginine (NOHA) (*21*, *22*). NOHA is an intermediate in

[†] This work was supported by National Institutes of Health Grants GM49758 (D.W.C.) and GM67788 (D.E.A.) and National Science Foundation Grant MCB0196103 (R.E.V.). E.C. was supported in part by the U.S. Army Medical Research and Materiel Command's Office of the Congressionally Directed Medical Research Programs through a Department of Defense Breast Cancer Research Predoctoral Fellowship.

[‡] Atomic coordinates of arginase complexes have been deposited in the Research Collaboratory for Structural Bioinformatics (http://www.rcsb.org/pdb) with the following accession codes: complex with fluoride ions and L-arginine, 1T5G; complex with L-valine, 1T4S; complex with dinor-N^{ω}-hydroxy-L-arginine, 1T4T; complex with descarboxy-nor-N^{ω}-hydroxy-L-arginine, 1T4R; and complex with dehydro-2(*S*)-amino-6-boronohexanoic acid, 1T4P.

* To whom correspondence should be addressed. Tel: (215) 898-5714. Fax: (215) 573-2201. E-mail: chris@xtal.chem.upenn.edu.

[§] University of Pennsylvania.

[||] Current address: Cambridge Institute for Medical Research, University of Cambridge, Hills Road, Cambridge CB2 2XY, U.K.

[⊥] Université Paris V.

[#] University of Toledo.

[▽] Current address: Department of Molecular Biology, The Scripps Research Institute, La Jolla, CA 92037.

[@] Temple University.

10.1021/bi0491705 CCC: $27.50
Published on Web 06/25/2004

Table 1: Arginase Inhibitors

Inhibitors	Structure	IC_{50} (pH 7.4)[a]	IC_{50} (pH 9.0)[a]
Fluoride[b]	F^-	1500 ± 200	8000 ± 2000
L-valine		650 ± 50	2300 ± 100
NOHA[c]	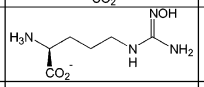	20 ± 2	
nor-NOHA[c]	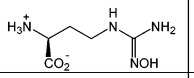	0.8 ± 0.2	1.5 ± 0.3
descarboxy-nor-NOHA[d]	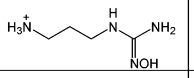	300 ± 50	450 ± 50
desamino-nor-NOHA[d]	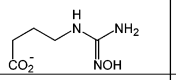	≥ 5000	> 5000
dinor-NOHA[c]	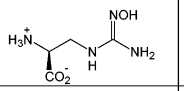	40 ± 10	400 ± 50
ABH[e]	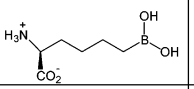	1.6 ± 0.8	18 ± 8
descarboxy-ABH[e]	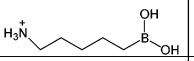	3000 ± 500	> 5000
dehydro-ABH[e]	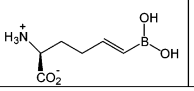	15 ± 5	65 ± 15

[a] IC_{50} values (in μM) were determined by testing each compound at eight concentrations and are means of at least four separate experiments. Rat liver arginase activity was measured by monitoring the conversion of [guanidino-^{14}C]-L-arginine to [^{14}C]urea in the presence of a final concentration of 20 mM L-arginine, as described in Materials and Methods. [b] Ref *13*. [c] Ref *30*. [d] Ref *31*. [e] Ref *38*.

the nitric oxide synthase-catalyzed oxidation of L-arginine to L-citrulline and nitric oxide (*23*−*26*), and it is also a competitive inhibitor of arginase with $K_i = 10-42$ μM (*21*, *22*, *27*). Modified analogues of NOHA have been synthesized (*27*−*29*) with striking structure−activity relationships: N^{ω}-hydroxy-nor-L-arginine (nor-NOHA) (*27*) is the most potent analogue with $IC_{50} = 0.8$ μM (*30*). X-ray crystal structures of NOHA and nor-NOHA complexed with arginase I show that the guanidinium hydroxyl group of each compound displaces the metal-bridging hydroxide ion of the native enzyme and asymmetrically bridges the binuclear manganese cluster (*31*). The binding of *S*-(2-sulfonamidoethyl)-L-cysteine (SEC; $K_d = 52.0$ μM) similarly displaces the metal-bridging hydroxide ion but in this case with an ionized sulfonamide NH^- group (*32*). Clearly, the exploitation of effective coordination interactions with the metal cluster is critical for inhibitor affinity.

The best inhibitor of arginase known to date is the reactive substrate analogue 2(*S*)-amino-6-boronohexanoic acid (ABH, $K_d = 0.11$ μM against rat arginase I; $K_i = 8.5$ nM against human arginase II) (*33*, *34*). The structure of the arginase I-ABH complex (*35*) shows that the trigonal planar boronic acid moiety of ABH undergoes nucleophilic attack by the metal-bridging hydroxide ion to yield a tetrahedral boronate anion: one boronate hydroxyl group symmetrically bridges $Mn^{2+}{}_A$ and $Mn^{2+}{}_B$, and a second boronate hydroxyl group coordinates to a site on $Mn^{2+}{}_A$ found vacant in the native enzyme. The same coordination chemistry accompanies the binding of *S*-(2-boronoethyl)-L-cysteine (BEC) to arginase I ($K_d = 2.22$ μM) (*36*) and arginase II ($K_i = 30$ nM) (*34*, *37*). Accordingly, the binding modes of ABH and BEC mimic the binding of the tetrahedral intermediate and its flanking transition states in catalysis. Interestingly, the introduction of a double bond between Cδ and Cϵ yields a more weakly binding inhibitor (designated dehydro-ABH) with $IC_{50} = 15$ μM (*38*).

Arginase inhibitors can enhance the bioavailability of L-arginine to nitric oxide (NO) synthase, and we have demonstrated that the arginase inhibitors ABH and BEC enhance nitric oxide-dependent smooth muscle relaxation in penile corpus cavernosum *ex vivo* (*35*, *36*) and erection and genital engorgement in the male and female genitalia *in vivo* (*37*). Accordingly, arginase inhibitors are potentially useful in the treatment of certain sexual arousal disorders. This pharmaceutical importance motivates the search for new amino acid inhibitors bearing different side-chain functional groups. We now report crystal structures of the complexes between arginase I and L-valine, dinor-NOHA, descarboxy-nor-NOHA, and dehydro-ABH (Table 1). We also report the first crystal structure of an arginase containing an intact $Mn^{2+}{}_2$ cluster bound to substrate L-arginine and two F^- ions. These structures reveal novel interactions that illuminate new aspects of coordination chemistry in the $Mn^{2+}{}_2$ cluster, thereby providing possible clues regarding new targets for inhibitor design efforts.

MATERIALS AND METHODS

Synthesis of Arginase Inhibitors. The dihydrochloride salts of N^{ω}-hydroxy-nor-L-arginine (nor-NOHA) and N^{ω}-hydroxy-dinor-L-arginine (dinor-NOHA) were synthesized as described previously (*30*). ABH and dehydro-ABH were obtained using previously described protocols (*38*).

Synthesis of 1-Amino-3-hydroxyguanidinopropane (Descarboxy-nor-NOHA). Descarboxy-nor-NOHA was obtained from 1,3-diamino propane by the following sequence of reactions. Treatment of 1,3-diamino propane with 1 equiv of di-*tert*-butylpyrocarbonate, $(Boc)_2O$, offered the mono-protected NH−Boc derivative. Addition of BrCN to this compound formed a cyanamide on the unprotected NH_2 group. Further addition of hydroxylamine hydrochloride to intermediate cyanamide resulted in the formation of a mixture of NH−Boc protected *N*-hydroxyguanidine and NH−Boc protected urea that was separated by column chromatography over SiO_2 (70:30:1 ethyl acetate/ethanol/acetic acid). Further deprotection of the NH−Boc protected *N*-hydroxyguanidine by treatment with anhydrous HCl in dioxane gave the dihydrochloride salt of descarboxy-nor-NOHA as an oil. Thin-layer chromatography performed on Merck silica gel 60 F_{254} glass plates with descarboxy-nor-NOHA dissolved in 2:1:2:2 acetone/water/2-propanol/acetic acid indicated a single spot with $R_f = 0.41$. ^{1}H NMR (D_2O): δ 2.04 (q, 2H, $J = 7.2$), 3.11 (t, 2H, $J = 7.2$), 3.38 (t, 2H, $J = 7.2$). ^{13}C NMR (D_2O): δ 29.1, 39.7, 41.0, 169.6; MS (FAB) 133 ($M + H^+$).

Synthesis of 4-(N-Hydroxyguanidino)-butyric Acid (Desamino-nor-NOHA). Desamino-nor-NOHA was obtained from 4-(*N*-benzyloxycarbonylamino)butyric acid (Novabiochem) that was protected as its *tert*-butyl ester using a previously

Table 2: Data Collection and Refinement Statistics

arginase ligand(s)	dehydro-ABH	descarboxy-nor-NOHA	dinor-NOHA	L-valine	L-arginine-$F^{-}{}_2$
resolution (Å)	2.6	2.6	2.2	2.8	2.4
unit cell parameters (Å)	$a = b = 88.4$ $c = 110.5$	$a = b = 88.3$ $c = 113.2$	$a = b = 88.3$ $c = 113.1$	$a = b = 87.8$ $c = 110.5$	$a = b = 87.72$ $c = 104.0$
total reflections	175920	242701	346597	121030	167380
completeness (%)[a]	93.5 (91.7)	95.8 (85.4)	92.0 (86.7)	99.6 (100)	99.9 (99.6)
R_{merge} (last shell)[a,b]	0.073 (0.240)	0.061 (0.189)	0.049 (0.176)	0.077 (0.422)	0.065 (0.119)
reflections used in refinement/test set	27963/2771	29877/2985	43094/4372	23147/1122	35725/1809
R_{cryst}[c]	0.264	0.255	0.258	0.258	0.228
R_{free}[c]	0.292	0.291	0.281	0.292	0.254
rms deviations					
bonds (Å)	0.010	0.013	0.009	0.009	0.006
angles (deg)	1.5	1.5	1.4	1.4	1.3
dihedral angles (deg)	23.8	23.9	22.4	23.2	22.8
improper dihedral angles (deg)	1.2	1.0	0.8	1.1	0.9
PDB accession code	1T4P	1T4R	1T4T	1T4S	1T5G

[a] Numbers in parentheses refer to the outer 0.1 Å shell of data. [b] R_{merge} for replicate reflections, $R = \Sigma|I_h - \langle I_h\rangle|/\Sigma\langle I_h\rangle$; I_h = intensity measured for reflection h; and $\langle I_h\rangle$ = average intensity for reflection h calculated from replicate data. [c] Crystallographic R factor, $R_{cryst} = \Sigma||F_o| - |F_c||/\Sigma|F_o|$ for reflections contained in the working set. Free R factor, $R_{free} = \Sigma||F_o| - |F_c||/\Sigma|F_o|$ for reflections contained in the test set held aside during refinement (5% of total). $|F_o|$ and $|F_c|$ are the observed and calculated structure factor amplitudes, respectively.

described protocol (*28*). Hydrogenolysis of NH-benzyloxycarbonyl *tert*-butyl ester in the presence of Pd/C quantitatively led to the unstable amine that was immediately reacted with BrCN to give the corresponding cyanamide. Further addition of hydroxylamine hydrochloride resulted in the formation of *N*-hydroxyguanidine and urea that were separated by column chromatography over SiO_2 (70:30:1 ethyl acetate/ethanol/acetic acid). Deprotection of the *tert*-butyl ester by treatment with anhydrous HCl in dioxane gave the hydrochloride salt of desamino-nor-NOHA as an oil. Thin-layer chromatography performed under the previous conditions indicated a single spot with $R_f = 0.70$. ^{1}H NMR (D_2O): δ 2.05 (qt, 2H, $J = 7.1$), 3.25 (t, 2H, $J = 7.3$), 3.45 (t, 2H, $J = 6.9$). ^{13}C NMR (D_2O): δ 28.9, 39.8, 41.1, 162.5, 182.7; MS (FAB) 162 ($M + H^+$).

Arginase Assays. Assays quantitating the [^{14}C]urea were produced from [guanidino-^{14}C]-L-arginine following a previously described method (*13*, *27*). A typical assay was performed in 100 μL of 0.2 M Tris-HCl buffer containing 20 mM L-arginine, 0.1 μCi [guanidino-^{14}C]-L-arginine, and variable concentrations of inhibitor. The reactions were initiated by the addition of purified rat liver arginase, and protein amounts were adjusted to yield less than 15% substrate conversion. After 10 min at 37 °C, 150 μL of cold stop buffer (0.25 M AcOH and 7 M urea) were added, and [^{14}C]urea was separated from unreacted [guanidino-^{14}C]-L-arginine by mixing with 250 μL of a slurry of Dowex AG-50W-X8 (H^+ form in stop buffer) and centrifugation. Aliquots of the supernatants were then counted after addition of Pico-Fluor 40. Fluoride inhibition of arginase at pH 9.0 (200 mM Na^+−CHES) was evaluated using the radioactive assay as described previously.

Crystallography. Recombinant wild-type rat arginase I was expressed in *E. coli* and purified by modification of previously described procedures (*39*). The C119A/ C168A/ C303A/H141A/Q19C arginase variant was prepared by modification of previously described procedures (*39*). The plasmid was then transformed into *E. coli* BL21(DE3) cells. Purification of the arginase variant was performed following the published procedure (*39*). This variant was then chemically modified at C19 with 3-bromopropylamine and is designated BPA-arginase I. Activity assays of BPA-arginase I yield K_M and k_{cat} values of 0.4 mM and 0.55 s^{-1}, respectively, indicating 0.22% of wild-type activity (K_M for wild-type (*39*) is 1.4 mM, and k_{cat} is 250 s^{-1}). We hypothesized that it would be easier to trap an L-arginine−fluoride complex in the active site of arginase I due to the significant activity loss measured for this variant.

Wild-type arginase I and BPA-arginase I were crystallized using the hanging drop vapor diffusion method as previously described (*7*). Briefly, a 3 μL drop of precipitant solution (50 mM bicine (pH 8.3−8.5), 12−18% PEG 8000, 2 mM $MnCl_2$) was added to a 3 μL drop of wild-type arginase I protein solution (16−18 mg/mL arginase I, 50 mM bicine (pH 8.5), 2 mM $MnCl_2$) on a silanized cover slip at 4 °C. Alternatively, a 3 μL drop of precipitant solution (50 mM bicine (pH 8.2−8.5), 20−24% PEG 8000, 2−5 μM $MnCl_2$) was added to a 3 μL drop of BPA-arginase I protein solution (10−16 mg/mL BPA-arginase I, 50 mM bicine (pH 8.5), 100 μM $MnCl_2$) on a silanized cover slip subsequently inverted and sealed over a 1 mL reservoir of precipitant buffer at room temperature. Crystals appeared after 4 weeks and belonged to space group $P3_2$ with unit cell parameters listed in Table 2. Enzyme−inhibitor complexes were prepared by soaking arginase I crystals for 3−8 days in 18% PEG 8000, 100 mM bicine (pH 8.5), 3 mM $MnCl_2$, and 5 mM inhibitor. Crystal-soaking solutions were changed twice daily. The BPA-arginase I−L-arginine−fluoride complex was prepared by soaking BPA-arginase I crystals in 26% PEG 8000, 50 mM bicine (pH 8.2−8.5), 100 μM $MnCl_2$, and 30 mM sodium fluoride for 2 days. The soaking solution was changed twice daily. After 2 days, these crystals were soaked in 26% PEG 8000, 50 mM bicine (pH 8.2−8.5), 100 μM $MnCl_2$, 30 mM sodium fluoride, and 10 mM L-arginine for 3 days. The crystal-soaking solution was changed thrice daily.

Prior to data collection, all crystals were gradually transferred to a cryoprotectant solution containing 30% glycerol in addition to the original precipitant solution and flash-cooled with liquid nitrogen. X-ray diffraction data for arginase-dinor NOHA, arginase-descarboxy-nor-NOHA, and arginase-dehydro-ABH were collected on a CCD detector at the Advanced Photon Light Source beamline 19-ID at the

Argonne National Laboratory (Argonne, IL). Diffraction data from the arginase I−L-valine complex were collected on a Mar 345 mm image plate detector at Stanford Synchrotron Radiation Laboratory beamline 7-1 at the Stanford Linear Accelerator Center in Menlo Park, CA. X-ray diffraction data for the arginase-L-arginine-fluoride complex were collected at the Advance Light Source, beamline 5.0.1. For each enzyme−inhibitor complex, intensity data integration and reduction were performed using the HKL suite of programs (*40*). Initial phases were determined by molecular replacement with the program AmoRe (*41*, *42*), using the trimer of native rat liver arginase I as a search model (*8*). Iterative rounds of refinement and rebuilding of the native model were performed using the programs CNS (*43*) and O (*44*), respectively. Each inhibitor was built into a simulated annealing omit electron density map in the final stages of refinement. Strict noncrystallographic symmetry was employed at the beginning of each refinement and later relaxed to appropriately weighted constraints as judged by R_{free}. Refinement statistics are reported in Table 2. Figures were generated using BOBSCRIPT and Raster3D (*45*, *46*). Atomic coordinates have been deposited in the Protein Data Bank (*47*) with accession codes listed in Table 2.

RESULTS

Inhibitory Effects Against Rat Arginase I. The inhibitory effects of the studied compounds toward rat arginase I have been previously reported (*13*, *27*−*31*, *33*, *38*). However, we report here their IC_{50} values measured under strictly identical conditions by quantifying the [^{14}C]urea produced from [guanidino-^{14}C]-L-arginine following a previously described protocol (*13*, *28*). The IC_{50} values were determined at pH 7.4 and 9.0 (where rat liver arginase displays its highest activity) and are presented in Table 1. The most potent inhibitors at both pH values are nor-NOHA and ABH; any modification of the α-amino acid functionalities of these compounds results in a dramatic loss of inhibitory activity. However, the loss of inhibitory activity of nor-NOHA is more sensitive to removal of the α-amino group in desamino-nor-NOHA than removal of the α-carboxylate in descarboxy-nor-NOHA. In addition, introducing a double bond between Cδ and Cϵ of ABH (in dehydro-ABH), or shortening the side chain of nor-NOHA (in dinor-NOHA), results in 10- and 40-fold losses of inhibitory activity, respectively. Inhibitors exhibit 2−5-fold enhanced inhibitory activity at pH 7.4 than at pH 9.0, except for dinor-NOHA and ABH that are 10-fold more active at pH 7.4 than at pH 9.0 (Table 1). The inhibition of arginase by ABH and nor-NOHA has been investigated in detail and involves different mechanisms (*28*, *31*, *34*, *35*). We have investigated arginase inhibition by dinor-NOHA at pH 7.4 and 9.0 and found that inhibition is fully reversible and competitive with substrate L-arginine, with K_i values of 35 and 380 μM at pH 7.4 and 9.0, respectively (Figure 1).

At pH 7.4, the F^- ion is a linear uncompetitive inhibitor of arginase (*13*). At pH 9.0 (the pH optimum of enzyme activity), the F^- ion is also an uncompetitive inhibitor of arginase, but replots of $1/K_{m,app}$ or $1/V_{max}$ as a function of [NaF] are nonlinear (Figure 2a). These results are consistent with partial uncompetitive inhibition and may indicate a more complex mode of interaction between the F^- ion and the enzyme (e.g., the binding of two F^- ions). The replot of $1/K_{m,app}$ as a function of $[NaF]^2$ is linear, which is consistent with the binding of two F^- ions (Figure 2b).

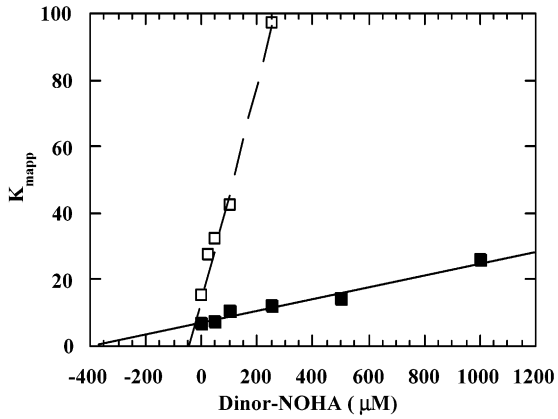

FIGURE 1: Determination of K_i values for rat arginase I inhibition by dinor-NOHA at pH 7.4 (□) and at pH 9.0 (■). Enzyme was incubated in the presence of increasing concentrations of L-arginine alone, and in the presence of differing concentrations of dinor-NOHA, to yield apparent K_m values. The replot of apparent K_m as a function of dinor-NOHA concentration gives a line that intercepts the *x*-axis at the K_i value. Data are representative of a typical experiment.

Structure of the BPA Arginase I−L-Arginine−Fluoride Complex. The structure of a BPA-modified arginase complex with L-arginine and fluoride was examined with the aim of trapping an intact substrate in the enzyme active site. Significantly, the crystal structure of this complex reveals that the unusual mode of uncompetitive inhibition involves the binding of two nonprotein ligands to the binuclear manganese cluster, both of which are interpreted as F^- ions. Metal-bound F^- ions are further stabilized by short hydrogen bond interactions with the positively charged guanidinium group of substrate L-arginine. Ligand binding does not trigger any major tertiary or quaternary structural changes, and the rms deviation of 314 Cα atoms is 0.26 Å between the structures of native arginase I and the BPA-arginase I−L-arginine−F^-_2 complex. The electron density map of Figure 3a reveals clear and unambiguous density for L-arginine in the arginase active site. With η-NH2····Mn^{2+} separations of 2.8−2.9 Å, L-arginine does not coordinate to the binuclear manganese cluster. The Mn^{2+}_A−Mn^{2+}_B separation is 3.3 Å, unchanged from that of the native enzyme. The Mn^{2+}_A ion is coordinated by H101 (Nδ1), D124 (Oδ1), D232 (Oδ2), D128 (Oδ1), and two F^- ions with distorted octahedral geometry. One F^- ion occupies the Mn^{2+}_A coordination site that is vacant in the native enzyme (*8*) and is 2.8 Å away from E277. The second F^- ion bridges Mn^{2+}_A and Mn^{2+}_B with separations of 2.4 and 2.2 Å, respectively, and the Mn^{2+}_B coordination polyhedron is completed by D124 (Oδ2), H126 (Nδ1), D232 (Oδ1), and D234 (Oδ1 and Oδ2) with distorted octahedral geometry. Metal-bound F^- ions make short hydrogen bond interactions with L-arginine (η-NH_2·· ·F^- separations = 2.4 and 2.5 Å). These hydrogen bonds comprise the structural basis of uncompetitive inhibition (i.e., the requirement for substrate binding to stabilize inhibitor binding).

Intriguingly, electron paramagnetic resonance experiments indicate that the F^- ion interacts with the binuclear manganese cluster of arginase in the absence of substrate (*13*), but this mode of interaction cannot correspond to an inhibitory

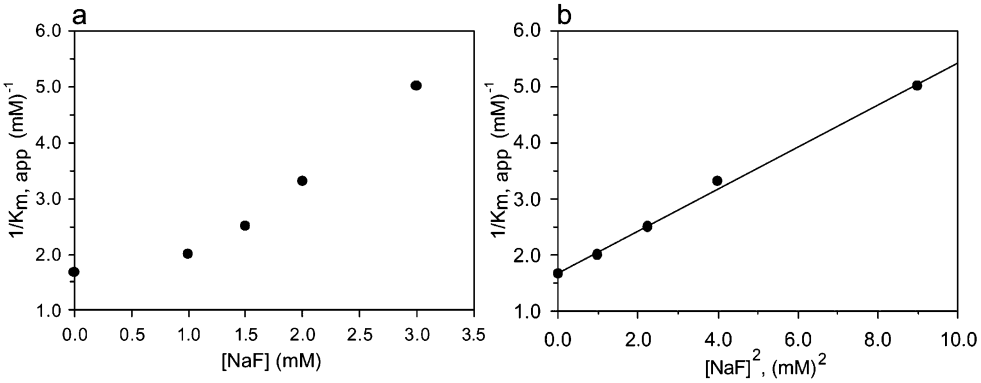

FIGURE 2: (a) Replot of $1/K_{m,app}$ as a function of [NaF] for the inhibition of arginase by the F^- ion at pH 9.0. (b) Replot of $1/K_{m,app}$ as a function of $[NaF]^2$ for the inhibition of arginase by the F^- ion at pH 9.0. The linearity of this plot is interpreted to indicate the binding of two F^- ions.

binding mode for a purely uncompetitive inhibitor. Perhaps a F^- ion binds weakly to the vacant coordination site on $Mn^{2+}{}_A$ in the native enzyme, but this binding mode does not cause measurable inhibition. The extra positive charge and hydrogen bonding opportunities afforded by L-arginine binding might stabilize the $F^-\cdots Mn^{2+}{}_A$ interaction as well as facilitate the subsequent displacement of the metal-bridging hydroxide ion by an inhibitory F^- ion. Such a scenario could explain why F^- ion binds more tightly at acidic pH, as it would be easier to displace a metal-bridging water molecule than a metal-bridging hydroxide ion (*13*).

We note that although the fluoride and hydroxide ions are isoelectronic and would be essentially indistinguishable in the electron density map (Figure 3a), the fact that electron paramagnetic resonance experiments indicate the binding of F^- ion to the $Mn^{2+}{}_2$ cluster (*13*) supports the assignment of F^- binding to the $Mn^{2+}{}_A$ site; the fact that an intact L-arginine molecule is bound suggests that the reactive nucleophile, metal-bridging hydroxide ion, has been replaced by an inert F^- ion that cannot attack the substrate. The binding of two F^- ions at high pH is also consistent with the kinetic replots in Figure 2.

The molecular recognition of the substrate L-arginine differs from that inferred from the binding of the reactive substrate analogue ABH (*35*). An anomalous substrate binding interaction might be expected in the presence of an uncompetitive inhibitor. The α-amino group of L-arginine hydrogen bonds to a solvent molecule, which in turn hydrogen bonds to D183 Oδ1 and D181 Oδ1 (Figure 3b). One of the α-carboxylate oxygen atoms of L-arginine accepts a hydrogen bond from a solvent molecule. This solvent molecule hydrogen bonds to the side-chain hydroxyl group and backbone NH group of S136. The other α-carboxylate oxygen accepts hydrogen bonds from N130 Nδ2 and two solvent molecules. One of these solvent molecules donates a hydrogen bond to the backbone carbonyl group of N139.

*Structure of the Arginase I−*L*-Valine Complex.* The binding of the inert amino acid L-valine does not cause any major changes in the tertiary or quaternary structure of arginase I. The rms deviation of 314 Cα atoms between the native and inhibitor complexed enzymes is 0.24 Å. An electron density map is found in Figure 4a. The $Mn^{2+}{}_A-Mn^{2+}{}_B$ separation is 3.1 Å, and $Mn^{2+}{}_A$ is coordinated by H101 (Nδ1), D124 (Oδ1), D232 (Oδ2), D128 (Oδ1), and a solvent molecule with distorted square pyramidal geometry, while $Mn^{2+}{}_B$ is coordinated by D124 (Oδ2), H126 (Nδ1), D232 (Oδ1), and D234 (Oδ1 and Oδ2) with distorted square pyramidal geometry (Figure 4b). The $Mn^{2+}{}_A$-bound solvent molecule is 2.7 Å away from $Mn^{2+}{}_B$, too long to be considered innersphere metal coordination. However, given the moderate resolution of this structure, the solvent molecule may be coordinated within experimental error. This solvent molecule in turn donates a hydrogen bond to D128. The α-amino and -carboxylate groups of L-valine occupy the same general positions as those of other arginase inhibitors with functionalized side chains such as NOHA (*31*) and ABH (*35*). The α-amino group of L-valine hydrogen bonds with D183 (Oδ2), N130, and a solvent molecule. This solvent molecule forms additional hydrogen bonds with the Oε2 carboxylate oxygen of E186 and the backbone carbonyl group of G142. The α-carboxylate moiety hydrogen bonds with a single solvent molecule that, in turn, hydrogen bonds with the side-chain hydroxyl group of T135 and the backbone carbonyl group of N139.

Structure of the Arginase I−Dinor-NOHA Complex. There are no major tertiary or quaternary changes in the arginase I−dinor-NOHA complex as compared with the arginase I−nor-NOHA complex (*31*) (the rms deviation of 314 Cα atoms between the two structures is 0.29 Å) and the arginase I−NOHA complex (*31*) (the rms deviation of 314 Cα atoms between the two structures is 0.34 Å). An electron density map is found in Figure 5a. The hydroxyl group of dinor-NOHA coordinates solely to $Mn^{2+}{}_B$. At a distance of 2.9 Å away from $Mn^{2+}{}_A$, the inhibitor hydroxyl group is too far from $Mn^{2+}{}_A$ to make an innersphere coordination interaction.

Surprisingly, a solvent molecule coordinates to $Mn^{2+}{}_A$ at the formerly vacant site observed in the native enzyme (*8*), which also corresponds to the binding site of one of the F^- ions in the L-arginine$-F^-{}_2$ complex (Figure 3). In the dinor-NOHA complex, the $Mn^{2+}{}_A$-bound solvent molecule donates a hydrogen bond to D128. Thus, in contrast to the binding of nor-NOHA and NOHA (*31*), the hydroxyl group of dinor-NOHA does not bridge the binuclear manganese cluster. Instead, by coordinating solely to $Mn^{2+}{}_B$, the inhibitor hydroxyl group bumps the metal-bridging hydroxide ion over to exclusive $Mn^{2+}{}_A$ coordination. That dinor-NOHA causes such structural changes in the binuclear manganese cluster while maintaining affinity comparable to that of NOHA (Table 1) is striking. The pH-dependent differences in IC_{50} and K_i values for *N*-hydroxyguanidine and F^- inhibitors

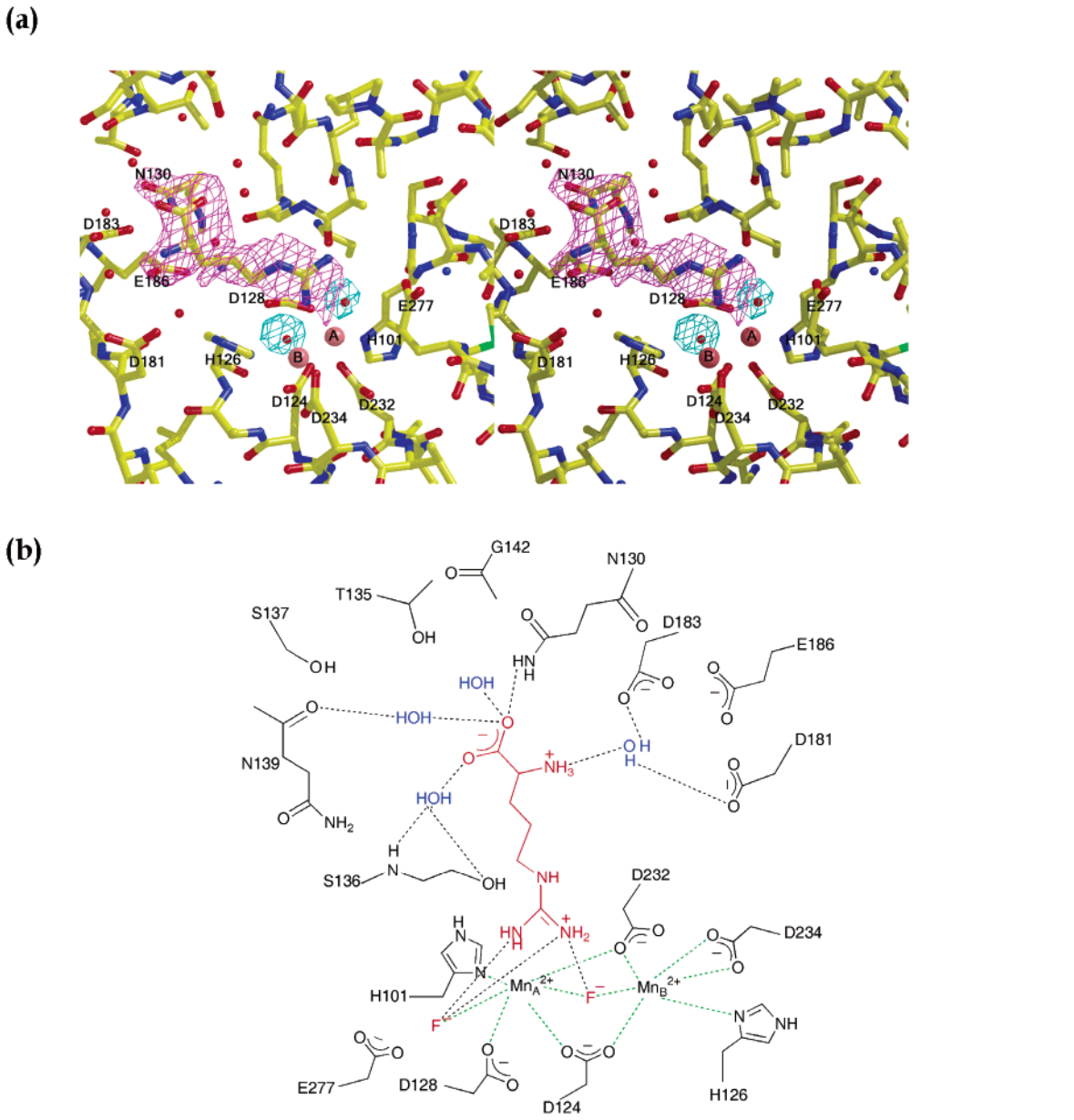

FIGURE 3: Arginase I−L-arginine-F^-_2 complex. (a) Omit electron density maps of the active site. The L-arginine omit map is contoured at 3.5σ, and the fluoride ion omit maps are contoured at 4σ. Selected active site residues are indicated. Atoms are color-coded as follows: C = yellow, O = red, and N = blue; manganese ions appear as light pink spheres, and fluoride ions appear as red spheres. (b) Summary of intermolecular interactions. Manganese coordination interactions are designated by green dashed lines, and hydrogen bonds are indicated by black dashed lines.

generally indicate tighter binding at pH 7.4 than pH 9.0 (Table 1 and Figure 1). Accordingly, the movement of the metal-bridging solvent molecule by these inhibitors may be easier to achieve at lower pH values where the H_2O form likely predominates, rather than at higher pH values where the HO^- form predominates. The activity-linked pK_a value of 7.9 likely corresponds to the ionization of the metal-bridging solvent molecule (*3*, *4*, *48*).

The $Mn^{2+}{}_A$−$Mn^{2+}{}_B$ separation is 3.4 Å. The $Mn^{2+}{}_A$ ion is coordinated by H101 (Nδ1), D124 (Oδ1), D128 (Oδ1), D232 (Oδ1), and a solvent molecule with distorted square planar geometry. The $Mn^{2+}{}_B$ ion is coordinated by H126 (Nδ1), D232 (Oδ1), D124 (Oδ2), D234 (Oδ1 and Oδ2), and the hydroxyl group of dinor-NOHA with distorted octahedral geometry (Figure 5). The ϵ-NH_2 group of dinor-NOHA donates a hydrogen bond to the side-chain hydroxyl group of T246. The γ-NH group hydrogen bonds with a solvent molecule.

The α-amino moiety of dinor-NOHA donates hydrogen bonds to D183 (Oδ2), E186 (Oϵ1), and two solvent molecules. One of these solvent molecules forms additional hydrogen bonds with G142 and E186, while the other solvent molecule hydrogen bonds to D181. One of the α-carboxylate oxygens hydrogen bonds with N130, while the other accepts a hydrogen bond from a solvent molecule that in turn hydrogen bonds with H141 (Nϵ2). This hydrogen bonding network is comparable to that observed in the arginase I-nor-NOHA complex and is more extensive than that observed in the arginase I−NOHA complex (*31*), but the modest resolution of these two structures may obscure the observation of some hydrogen bonds, especially those involving solvent atoms. Nevertheless, the extensive hydrogen bonding

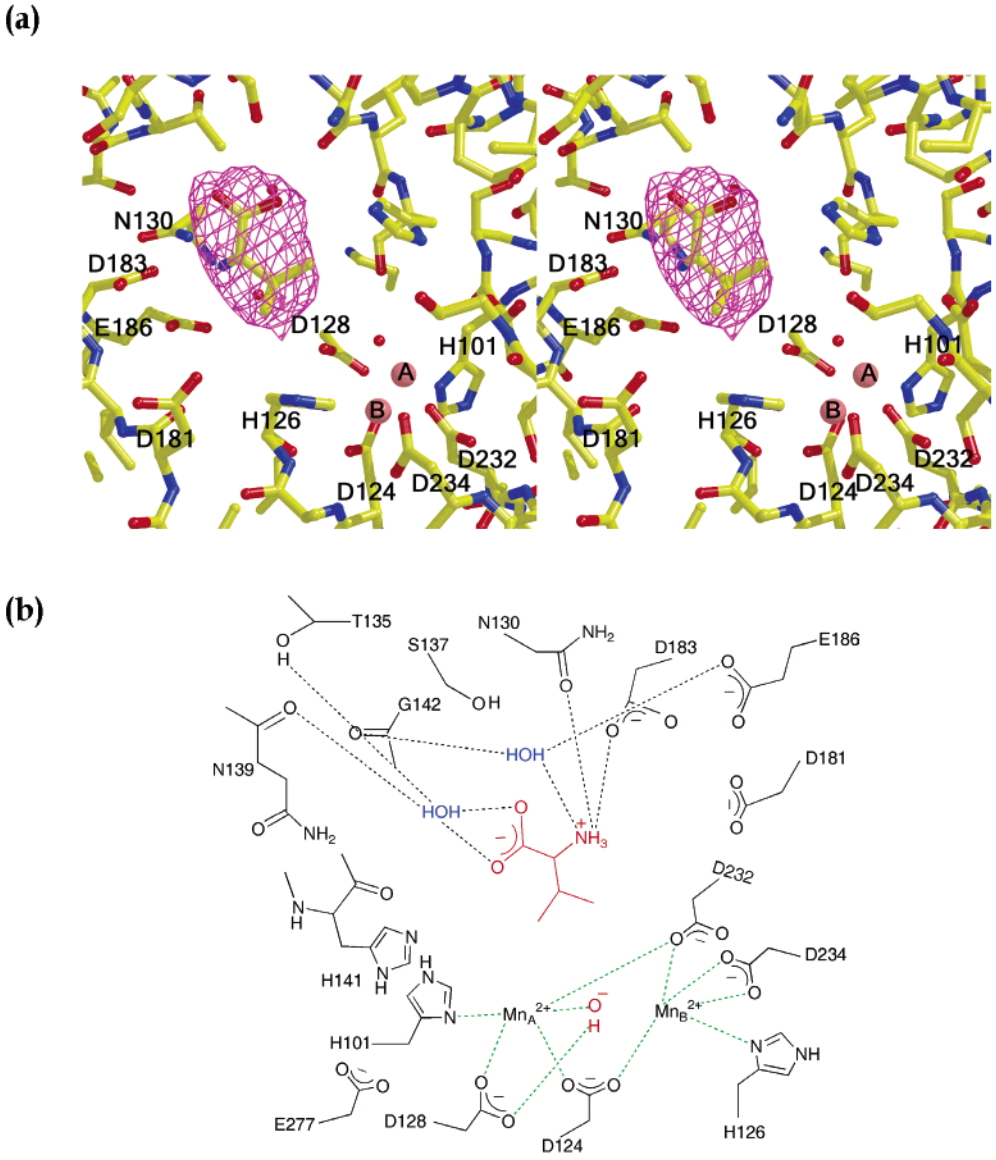

FIGURE 4: Arginase I−L-valine complex. (a) Omit electron density map contoured at 6.4σ; selected active site residues are indicated. Atoms are color-coded as follows: C = yellow, O = red, and N = blue; manganese ions appear as light pink spheres, and water molecules appear as red spheres. (b) Summary of intermolecular interactions. Manganese coordination interactions are designated by green dashed lines, and hydrogen bonds are indicated by black dashed lines.

network that is observed may account for the relative retention of arginase I affinity for dinor-NOHA as compared to that for NOHA and nor-NOHA (Table 1).

Structure of the Arginase I−Descarboxy-nor-NOHA Complex. The binding of descarboxy-nor-NOHA to the active site of arginase I does not trigger any major tertiary or quaternary changes, and the rms deviation of 314 Cα atoms between the native and inhibitor-complexed enzymes is 0.28 Å. The hydroxyl oxygen of descarboxy-nor-NOHA displaces the metal-bridging hydroxide ion and asymmetrically coordinates to the binuclear manganese cluster with Mn^{2+}_A−O and Mn^{2+}_B−O separations of 2.3 and 2.5 Å, respectively (Figure 6). In the nor-NOHA complex (*31*), the corresponding separations are 2.5 and 2.6 Å, respectively, and the D232 side chain moves away from Mn^{2+}_A. In the descarboxy-nor-NOHA complex, D232 does not move: Mn^{2+}_A is coordinated by H101 (Nδ1), D128 (Oδ1), D124 (Oδ1), D232 (Oδ1), and the hydroxyl group of descarboxy-nor-NOHA with distorted square pyramidal geometry. A solvent molecule is located 2.8 Å away from Mn^{2+}_A, a distance too long to be considered innersphere metal coordination. However, given the moderate resolution of this structure, the solvent molecule may be coordinated within experimental error. The Mn^{2+}_B ion is coordinated by D232 (Oδ1), D124 (Oδ2), H126 (Nδ1), D234 (Oδ1 and Oδ2), and the hydroxyl group of descarboxy-nor-NOHA with distorted octahedral geometry. The Mn^{2+}_A−Mn^{2+}_B separation is 3.0 Å, shorter than the corresponding separation in the arginase I-nor-NOHA complex (3.5 Å) (*31*) or that in the native enzyme (3.3 Å) (*8*).

The hydroxyl group of descarboxy-nor-NOHA asymmetrically bridges the binuclear manganese cluster and appears to make a bifurcated hydrogen bond with D128 and a solvent molecule. The ξ-NH_2 group donates a hydrogen bond to the side-chain hydroxyl group of T246. The α-amino moiety of descarboxy-nor-NOHA hydrogen bonds to two solvent molecules. One of these solvent molecules hydrogen bonds with the S137 side chain and a solvent molecule, while the other solvent molecule hydrogen bonds with the backbone carbonyl groups of N139 and G142 (Figure 6b). The IC_{50} values of the descarboxy and desamino analogues (Table 1)

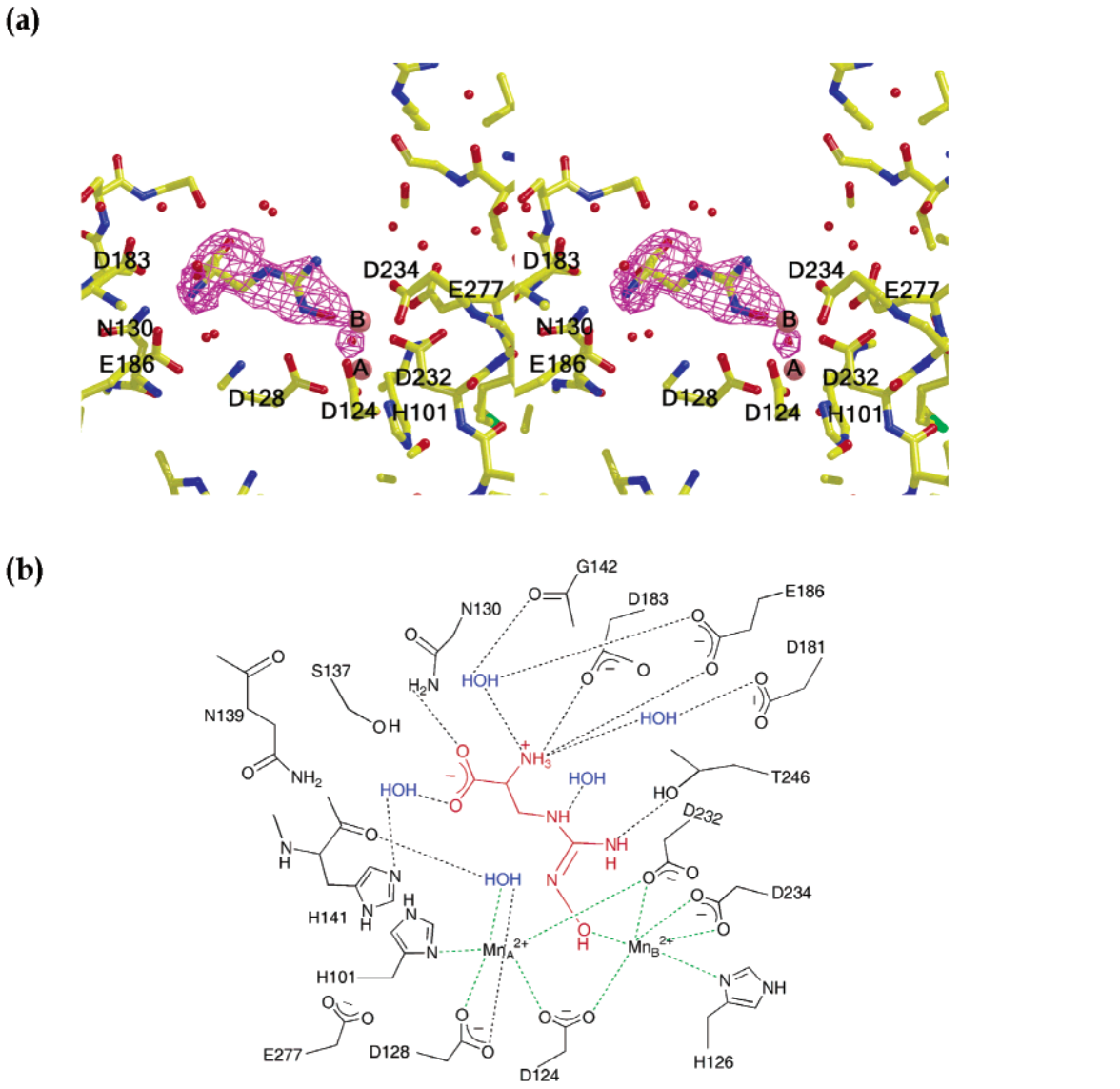

FIGURE 5: Arginase I−dinor-NOHA complex. (a) Omit electron density map contoured at 5.5σ; selected active site residues are indicated. Atoms are color-coded as follows: C = yellow, O = red, and N = blue; manganese ions appear as light pink spheres, and water molecules appear as red spheres. (b) Summary of intermolecular interactions. Manganese coordination interactions are designated by green dashed lines, and hydrogen bonds are indicated by black dashed lines.

show that inhibitor affinity is more sensitive to the deletion of the α-amino group than the α-carboxylate group. The direct hydrogen bonds with D183 and E186 made by the α-amino group of nor-NOHA (*31*) are not observed in the structure of the arginase−descarboxy-nor-NOHA complex. Instead, the α-amino group is positioned to form solvent-mediated hydrogen bonds with S137, G142, and N139.

Structure of the Arginase−Dehydro-ABH Complex. There are no major changes in the tertiary or quaternary structure of this complex, with the rms deviation of 308 Cα atoms being 0.33 Å between the arginase I−dehydro-ABH and arginase I−ABH complexes. A simulated annealing omit map (Figure 7) shows that the tetrahedral boronate anion group binds in a fashion similar to that of ABH (*35*). Boronate hydroxyl group O1 bridges the binuclear manganese cluster slightly asymmetrically (O1−Mn^{2+}_A separation = 2.2 Å, O1−Mn^{2+}_B separation = 2.0 Å) and donates a hydrogen bond to D128. Boronate hydroxyl group O2 makes a weak coordination interaction with Mn^{2+}_A (Mn^{2+}_A−O2 separation = 2.5 Å) and donates a hydrogen bond to the backbone carbonyl group of H141 and the carboxylate side chain of E277. Boronate hydroxyl group O3 hydrogen bonds with a solvent molecule.

The Mn^{2+}_A−Mn^{2+}_B separation is 3.3 Å, identical to that in the native enzyme (*8*). The Mn^{2+}_A ion is coordinated by D128 (Oδ1), D124 (Oδ1), H101 (Nδ1), D232 (Oδ1), and boronate hydroxyl groups O1 and O2 in distorted octahedral fashion (Figure 7). The Mn^{2+}_B ion is coordinated by D124 (Oδ2), H126 (Nδ1), D234 (Oδ1 and Oδ2), D232 (Oδ1), and boronate hydroxyl group O1 with distorted octahedral geometry.

The extensive hydrogen bond network with α-substituents observed in the arginase I−ABH complex (*35*) is retained to a certain degree in the arginase I−dehydro-ABH complex. The α-amino group hydrogen bonds to D183 (Oδ2) and a solvent molecule, which in turn hydrogen bonds to D183 and the backbone carbonyl group of D181. The α-carboxylate group O1 hydrogen bonds with N130 and a solvent molecule that in turn hydrogen bonds to the backbone carbonyl group of N139 (Figure 7b). The other α-carboxylate oxygen

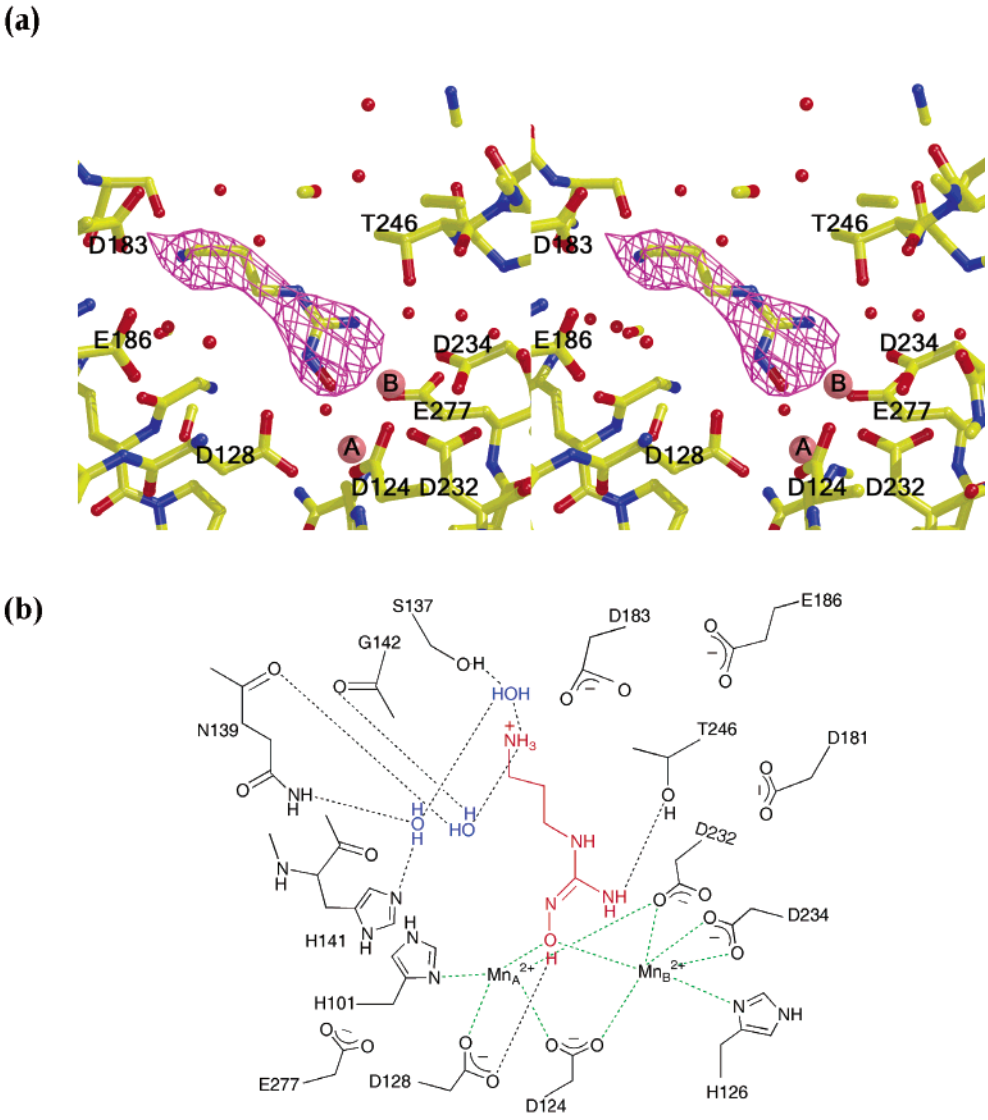

FIGURE 6: Arginase I−descarboxy-nor-NOHA complex. (a) Omit electron density map contoured at 3.2σ; selected active site residues are indicated. Atoms are color-coded as follows: C = yellow, O = red, and N = blue; manganese ions appear as light pink spheres, and water molecules appear as red spheres. (b) Summary of intermolecular interactions. Manganese coordination interactions are designated by green dashed lines, and hydrogen bonds are indicated by black dashed lines.

hydrogen bonds to S137 and a solvent molecule that forms an additional hydrogen bond with H141 (Nϵ2). Although the binding mode of unsaturated ABH is generally similar to that of ABH (*35*), subtle differences exist among the two structures, especially in the hydrogen bond interactions of the α-amino and α-carboxylate groups. These differences might arise from the geometric differences in the Cδ−Cϵ bond order between ABH and dehydro-ABH. Additionally, the α-substituents may engage in additional direct or solvent-mediated hydrogen bonds with the protein that remain unobserved due to the 2.6 Å resolution of this structure as compared with the 1.7 Å resolution of the arginase I−ABH structure (*35*).

The Cδ=Cϵ double bond in the dehydro-ABH side chain alters the distance between the α-amino and the α-carboxylate groups and the boronate anion. As affinity trends indicate with NOHA (*30*, *31*), nor-NOHA (*30*, *31*), dinor-NOHA (*30*), and with the hydroxylamines N^{ϵ}-hydroxy-L-lysine (*28*) and N^{δ}-hydroxy-L-ornithine (*28*), altering the side-chain length alters the affinity of amino acid inhibitors. The observed difference in the affinity of dehydro-ABH between pH 7.4 and 9.0 might arise due to the fact that at pH 7.4, the predominant form of the boronic acid is trigonal planar and is available for nucleophilic attack by the metal-bridging hydroxide ion; at pH 9.0, the tetrahedral boronate anion nearly predominates (the pK_a of ABH and its derivatives should be similar to that of BEC, which is 9.3) (*34*) and cannot undergo nucleophilic attack by the metal-bridging hydroxide ion.

DISCUSSION

Direct or solvent-mediated hydrogen bonds with the α-amino and -carboxylate groups of substrate or inhibitors are key affinity determinants in the arginase active site. Catalytic activity against alternative substrates is extremely sensitive to the presence or absence of unmodified α-substituents (*17*), and the high-resolution X-ray crystal structures of ABH bound to rat arginase I and L-arginine bound to inactivated arginase from *Bacillus caldovelox* first revealed that the molecular recognition of inhibitor α-substituents saturates the hydrogen bonding potential of these substituents (i.e., four hydrogen bonds donated to the α-carboxylate and

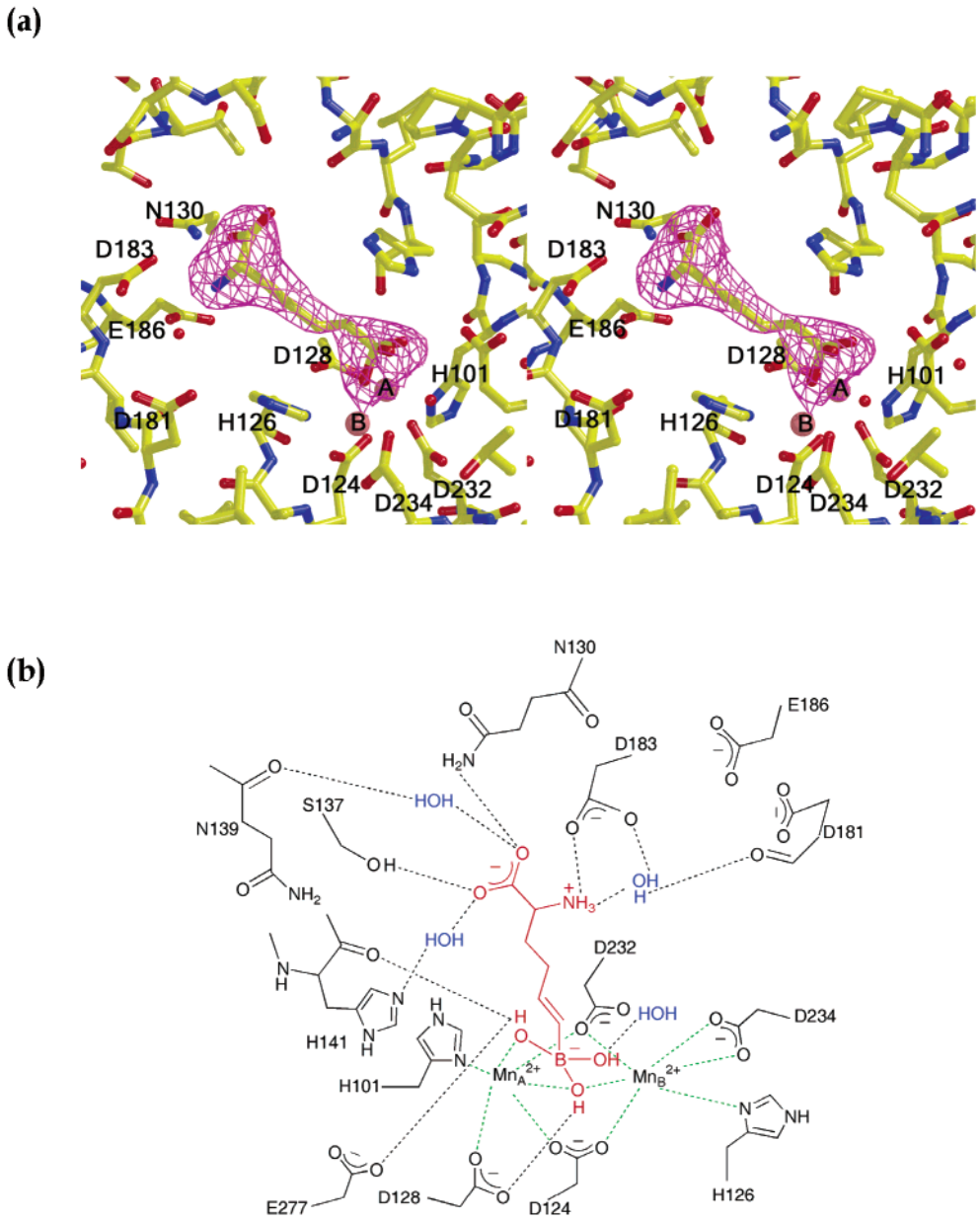

FIGURE 7: Arginase I−dehydro-ABH complex. (a) Omit electron density map contoured at 5.5σ; selected active site residues are indicated. Atoms are color-coded as follows: C = yellow, O = red, and N = blue; manganese ions appear as light pink spheres, and water molecules appear as red spheres. (b) Summary of intermolecular interactions. Manganese coordination interactions are designated by green dashed lines, and hydrogen bonds are indicated by black dashed lines.

three hydrogen bonds accepted from the α-amino group) (*35*, *49*). Given the array of structural information now available regarding the binding of substrate and amino acid inhibitors to bacterial arginase (*49*), rat arginase I (*31*, *32*, *35*, *36*), and human arginase II (*37*), common themes emerge regarding the molecular recognition of α-substituents upon merging previously reported information with the wealth of structural results emanating from the current study.

First, the α-amino group of every amino acid inhibitor studied except for NOHA donates a hydrogen bond to the α-carboxylate group of D183 (the α-amino group of NOHA (*31*) interacts more closely with E186). In some arginase−inhibitor complexes, both D183 and E186 interact directly with the inhibitor α-amino group (L-ornithine (*31*), nor-NOHA (*31*), dinor-NOHA (Figure 5)), and in others the hydrogen bond interaction with E186 is bridged by a water molecule (ABH (*35*), BEC (*36*), and L-valine (Figure 4)). Water-mediated hydrogen bonds are observed between the α-amino group and the backbone carbonyl of G142 (ABH (*35*), BEC (*36*), L-valine (Figure 4), descarboxy-nor-NOHA (Figure 6)) and/or D181 (ABH (*35*), BEC (*36*), and dehydro-ABH (Figure 7)). That water-mediated interactions are not uniformly observed in all arginase−inhibitor complexes is probably a consequence of varying resolutions of the X-ray crystal structure determinations. Accordingly, we conclude that the tightest-binding inhibitors will exploit a direct α-amino hydrogen bond and salt-link interaction with D183, a direct or water-mediated interaction with E186, and a water-mediated interaction with the backbone of the carbonyl groups of G142 and/or D181. The direct interaction with D183 appears to be the most important, whereas the water-mediated hydrogen bonds appear to have more structural variability/flexibility. All of the residues involved in these interactions except for D181 (serine in bacterial arginase)

are conserved in bacterial arginase and human arginase II (*37*, *49*).

The molecular recognition of the α-carboxylate group appears to be dominated by two direct hydrogen bonds with protein residues: the N130 carboxamide NH_2 group donates a hydrogen bond to the α-carboxylate groups of ABH (*35*), BEC (*36*), L-ornithine (*31*), L-arginine (Figure 3), dinor-NOHA (Figure 5), and dehydro-ABH (Figure 7), and the S137 hydroxyl group donates a hydrogen bond to the α-carboxylate groups of ABH (*35*), BEC (*36*), L-ornithine (*31*), and dehydro-ABH (Figure 7). Water-mediated hydrogen bond interactions are observed with T135, N139, and H141 in several but not all complexes, which may again be due in part to the varying resolutions of the crystal structure determinations. Accordingly, we conclude that the tightest-binding inhibitors will exploit direct α-carboxylate hydrogen bond interactions with N130 and S137 and water-mediated interactions with T135, N139, and H141. All of these residues except for T135 (serine in bacterial arginase) are conserved in bacterial arginase and human arginase II (*37*, *48*). It is interesting that in contrast with the molecular recognition of the α-amino group, salt-link interactions do not play a role in α-carboxylate recognition. It is also interesting that inhibitor affinity appears to be more sensitive to the deletion of the α-amino group than the α-carboxylate group (Table 1). This is consistent with structure−activity relationships observed for the arginase-catalyzed hydrolysis of modified L-arginine substrates (*17*) as well as desamino and descarboxy analogues of the alternative substrate L-thioarginine (*50*).

Parenthetically, we note that the binding of L-arginine to arginase I appears to be somewhat perturbed by the binding of two F- ions to the binuclear manganese cluster. A slight reorganization of the α-substituents consequently alters interactions of the α-amino group (i.e., the hydrogen bond interaction with D183 becomes water-mediated instead of direct (Figure 3)). Also, we note that in the arginase I complex with *S*-(2-sulfonamidoethyl)-L-cysteine (SEC), the direct α-amino group-D183 hydrogen bond is preserved, but the α-carboxylate interaction with N130 is lost, and the α-carboxylate−S137 interaction becomes water-mediated (*32*). This may account for the weaker affinity of SEC relative to the boronic acid inhibitors ABH or BEC.

Certain aspects of manganese coordination chemistry should be highlighted for this series of enzyme−inhibitor complexes. First, the crystal structure of the arginase I−L-arginine−F^-_2 complex provides the first view of a μ-fluoro bridge in a Mn^{2+}_2 cluster in a protein, and it also provides the first view of substrate binding to an arginase containing an intact binuclear manganese cluster (Figure 3). Additionally, this structure provides a rare example of an enzyme complexed with an uncompetitive inhibitor and its biological substrate—that two F^- ions bind, one bridging and one terminal—is even more remarkable and also consistent with the data reported in Figure 2. Strong hydrogen bond interactions observed between the F^- ions and the guanidinium group of L-arginine provide a dramatically simple illustration of how interactions with the substrate stabilize the binding of an uncompetitive inhibitor. Given that fluoride inhibition is uncompetitive and not noncompetitive, it is likely that the binuclear manganese cluster, already liganded by four negatively charged aspartate residues, cannot accommodate the binding of two additional negatively charged fluoride ions without the electrostatic assistance of the positively charged guanidinium moiety of the substrate.

The coordination chemistry of the Mn^{2+}_A ion is especially notable in the binding of inhibitors. In native rat arginase I, Mn^{2+}_A is coordinated with square pyramidal geometry, thus leaving a vacant coordination site (*8*). This coordination site is occupied by a hydroxyl group of ABH and BEC and by a sulfonamide oxygen of SEC in the respective enzyme−inhibitor complexes (*32*, *35*, *36*). These coordination phenomena suggest that the vacant site on Mn^{2+}_A is important for the binding and stabilization of the tetrahedral intermediate and its flanking transition states. In other arginase I−inhibitor complexes, the vacant site on Mn^{2+}_A is occasionally occupied in a surprising fashion. In the complex with L-arginine−F^-_2, the Mn^{2+}_A site is occupied by one of the F^- ions, and in the complex with dinor-NOHA, a solvent molecule binds to this site while the inhibitor hydroxyl group interacts exclusively with Mn^{2+}_B. Thus, the Mn^{2+}_A site appears to be kept vacant for purposes of transition state stabilization in catalysis, but tight-binding inhibitors may exploit a coordination interaction at this site with beneficial consequences for affinity. It should be noted that this site is observed occupied by a water molecule in the native bacterial arginase structure (*49*). Moreover, smeared electron density is observed at this site in monomer C of native rat liver arginase (*51*). Therefore, the vacant site on Mn^{2+}_A may actually contain a weakly bound, poorly occupied water molecule that is nevertheless readily displaced for catalysis and inhibitor binding. It is likely that F^- can bind to the Mn^{2+}_A site in the absence of substrate, consistent with the results of electron paramagnetic resonance experiments (*13*).

On the basis of this structural work, a new class of arginase inhibitors can be considered to target the Mn^{2+}_A site alone and not the site corresponding to the metal-bridging hydroxide ion. Since coordination to the Mn^{2+}_A site occurs readily, and coordination to the bridging site is more difficult due to displacement of the tightly bound hydroxide ion, an alternative design strategy targeting interactions with the vacant Mn^{2+}_A site in the binuclear manganese cluster may lead to new types of inhibitors.

In closing, it is interesting to note that in the arginase I complexes with L-valine (Figure 4) and dinor-NOHA (Figure 5) the metal-bound solvent molecule makes an innersphere coordination interaction solely with Mn^{2+}_A. The loss of the metal-bridging solvent molecule may account for the disappearance of the binuclear electron paramagnetic resonance signal upon formation of the complex with L-valine (*20*). Whether inhibitor binding sterically requires the metal-bound solvent molecule to shift from a bridging coordination interaction to a terminal coordination interaction in the binuclear manganese cluster (e.g., as in the dinor-NOHA complex), or not (e.g., as in the L-valine complex), these complexes are among the first to reveal a metal cluster in arginase with only two bridging ligands. Site-specific variants of arginase I that perturb the coordination polyhedron of either Mn^{2+}_A or Mn^{2+}_B reveal that the metal-bridging solvent molecule of the native enzyme (*8*) shifts to a terminal coordination mode on the metal with the intact set of protein ligands (i.e., if a ligand to Mn^{2+}_A is perturbed, the solvent shifts to exclusive Mn^{2+}_B coordination, and vice versa (*52*)). Accordingly, this coordination chemistry may exemplify the

entactic state hypothesis, namely, that the enzyme stabilizes the metal coordination polyhedra in an energized or strained configuration, the energetic benefit of which is harnessed for catalysis upon substrate binding (*53*). Additional high-resolution structural studies of arginase I may further illuminate these aspects of coordination chemistry and catalysis.

ACKNOWLEDGMENT

We thank the Argonne National Laboratory, the Stanford Linear Accelerator Center, and the Advance Light Source for beamtime access.

REFERENCES

1. Jenkinson, C. P., Grody, W. W., and Cederbaum, S. D. (1996) Comparative properties of arginases, *Comp. Biochem. Physiol. B114*, 107−132.
2. Wu, G., and Morris, S. M., Jr. (1998) Arginine metabolism: nitric oxide and beyond, *Biochem. J. 336*, 1−17.
3. Christianson, D. W., and Cox, J. D. (1999) Catalysis by metal-activated hydroxide in zinc and manganese metalloenzymes, *Annu. Rev. Biochem. 68*, 33−57.
4. Ash, D. E., Cox, J. D., and Christianson, D. W. (2000) Manganese and its Role in Biological Systems, in *Metal Ions in Biological Systems* (Sigel, A., Sigel H., Eds.) Marcel Dekker, New York, Vol. 37, pp 407−428.
5. Morris, S. M., Jr. (2002) Regulation of enzymes of the urea cycle and arginine metabolism, *Annu. Rev. Nutr. 22*, 87−105.
6. Herzfeld, A., and Raper, S. M. (1976) The heterogeneity of arginases in rat tissues, *Biochem. J. 153*, 469−478.
7. Kanyo, Z. F., Chen, C. Y., Daghigh, F., Ash, D. E., and Christianson, D. W. (1992) Crystallization and oligomeric structure of rat liver arginase, *J. Mol. Biol. 224*, 1175−1177.
8. Kanyo, Z. F., Scolnick, L. R., Ash, D. E., and Christianson, D. W. (1996) Structure of a unique binuclear manganese cluster in arginase, *Nature 383*, 554−557.
9. Shi, O., Morris, S. M., Jr., Zoghbi, H., Porter, C. W., and O'Brien, W. E. (2001) Generation of a mouse model for arginase II deficiency by targeted disruption of the arginase II gene, *Mol. Cell. Biol. 21*, 811−813.
10. Buga, G. M., Singh, R., Pervin, S., Rogers, N. E., Schmitz, D. A., Jenkinson, C. P., Cederbaum, S. D., and Ignarro, L. J. (1996) Arginase activity in endothelial cells: inhibition by N^{ω}-hydroxy-L-arginine during high-output NO production, *Am. J. Physiol. 271*, H1988−H1998.
11. Chang, C. I., Liao, J. C., and Kuo, L. (1998) Arginase modulates nitric oxide production in activated macrophages, *Am. J. Physiol. 274*, H342−H348.
12. Boucher, J. L., Moali, C., and Tenu, J. P. (1999) Nitric oxide biosynthesis, nitric oxide synthase inhibitors, and arginase competition for L-arginine utilization, *Cell Mol. Life Sci. 55*, 1015−1028.
13. Pethe, S., Boucher, J.-L., and Mansuy, D. (2002) Interaction of anions with rat liver arginase: specific inhibitory effects of fluoride, *J. Inorg. Biochem. 88*, 397−402.
14. Lenti, C. (1945) Inhibition and reactivation of arginase, *Bull. Soc. Ital. Biol. Sper. 29*, 636−637.
15. Van Pilsum, J. F., Taylor, D., Zakis, B., and McCormick, P. (1970) Simplified assay for transamidinase activities of rat kidney homogenates, *Anal. Biochem. 35*, 277−286.
16. Tormanen, C. D. (2003) Substrate inhibition of rat liver and kidney arginase with fluoride, *J. Inorg. Biochem. 93*, 243−246.
17. Reczkowski, R. S., and Ash, D. E. (1994) Rat liver arginase: kinetic mechanism, alternate substrates, and inhibitors, *Arch. Biochem. Biophys. 312*, 31−37.
18. Fuentes, J. M., Campo, M. L., and Soler, G. (1994) Kinetics and inhibition by some amino acids of lactating rat mammary gland arginase, *Arch. Int. Physiol. Biochim. Biophys. 102*, 255−258.
19. Carvajal, N., and Cederbaum, S. D. (1986) Kinetics of inhibition of rat liver and kidney arginases by proline and branched-chain amino acids, *Biochim. Biophys. Acta 870*, 181−184.
20. Sossong, T. M., Khangulov, S. V., Cavalli, R. C., Soprano, D. R., Dismukes, G. C., and Ash, D. E. (1997) Catalysis on dinuclear Mn(II) centers: Hydrolytic and redox activities of rat liver arginase, *J. Biol. Inorg. Chem. 2*, 433−443.
21. Daghigh, F., Fukuto, J. M., and Ash, D. E. (1994) Inhibition of rat liver arginase by an intermediate in NO biosynthesis, N^{ω}-hydroxy-L-arginine: implications for the regulation of nitric oxide biosynthesis by arginase, *Biochem. Biophys. Res. Commun. 202*, 174−180.
22. Boucher, J.-L., Custot, J., Vadon, S., Delaforge, M., Lepoivre, M., Tenu, J.-P., Yapo, A., and Mansuy, D. (1994) N^{ω}-hydroxyl-L-arginine, an intermediate in the L-arginine to nitric oxide pathway, is a strong inhibitor of liver and macrophage arginase, *Biochem. Biophys. Res. Commun. 203*, 1614−1621.
23. Stuehr, D. J., Kwon, N. S., Nathan, C. F., Griffith, O. W., Feldman, P. L., and Wiseman, J. (1991) N^{ω}-hydroxy-L-arginine is an intermediate in the biosynthesis of nitric oxide from L-arginine, *J. Biol. Chem. 266*, 6259−6263.
24. Pufahl, R. A., Nanjappan, P. G., Woodard, R. W., and Marletta, M. A. (1992) Mechanistic probes of N-hydroxylation of L-arginine by the inducible nitric oxide synthase from murine macrophages, Biochemistry *31*, 6822−6828.
25. Klatt, P., Schmidt, K., Uray, G., and Mayer, B. (1993) Multiple catalytic functions of brain nitric oxide synthase. Biochemical characterization, cofactor-requirement, and the role of N^{ω}-hydroxy-L-arginine as an intermediate, *J. Biol. Chem. 268*, 14781−14787.
26. Kerwin, J. F., Lancaster, J. R., and Feldman, P. L. (1995) Nitric oxide: a new paradigm for second messengers, *J. Med. Chem. 38*, 4343−4362.
27. Custot, J., Moali, C., Brollo, M., Boucher, J.-L., Delaforge, M., Mansuy, D., Tenu, J. P., and Zimmermann, J. L. (1997) The new α-amino acid N^{ω}-hydroxy-nor-L-arginine: a high-affinity inhibitor of arginase well-adapted to bind to its manganese cluster, *J. Am. Chem. Soc. 119*, 4086−4087.
28. Custot, J., Boucher, J.-L., Vadon, S., Guedes, C., Dijols, S., Delaforge, M., and Mansuy, D. (1996) N^{ω}-hydroxyamino-α-amino acids as a new class of very strong inhibitors of arginases, *J. Biol. Inorg. Chem. 1*, 73−82.
29. Vadon, S., Custot, J., Boucher, J.-L., and Mansuy, D. (1996) Synthesis and effects on arginase and nitric oxide synthase of two novel analogues of N^{ω}-hydroxyarginine, N^{ω}-hydroxyindospicine, and *p*-hydroxyamidinophenylalanine, *J. Chem. Soc., Perkin Trans. 1*, 645−648.
30. Moali, C., Brollo, M., Custot, J., Sari, M.-A., Boucher, J.-L., Stuehr, D. J., and Mansuy, D. (2000) Recognition of α-amino acids bearing various C═NOH functions by nitric oxide synthase and arginase involves very different structural determinants, *Biochemistry 39*, 8208−8218.
31. Cox, J. D., Cama, E., Colleluori, D. M., Pethe, S., Boucher, J.-L., Mansuy, D., Ash, D. E., and Christianson, D. W. (2001) Mechanistic and metabolic inferences from the binding of substrate analogues and products to arginase, *Biochemistry 40*, 2689−2701.
32. Cama, E., Shin, H., and Christianson, D. W. (2003) Design of amino acid sulfonamides as transition-state analogue inhibitors of arginase, *J. Am. Chem. Soc. 125*, 13052−13057.
33. Baggio, R., Elbaum, D., Kanyo, Z. F., Carroll, P. J., Cavalli, R. C., Ash, D. E., and Christianson, D. W. (1997) Inhibition of Mn^{2+}_2-arginase by borate leads to the design of a transition state analogue inhibitor, 2(*S*)-amino-6-boronohexanoic acid, *J. Am. Chem. Soc. 119*, 8107−8108.
34. Colleluori D. M., and Ash, D. E. (2001) Classical and slow-binding inhibitors of human type II arginase, *Biochemistry 40*, 9356−9362.
35. Cox, J. D., Kim, N. N., Traish, A. M., and Christianson, D. W. (1999) Arginase-boronic acid complex highlights a physiological role in erectile function, *Nat. Struct. Biol. 6*, 1043−1047.
36. Kim, N. N., Cox, J. D., Baggio, R. F., Emig, F. A., Mistry, S. K., Harper, S. L., Speicher, D. W., Morris, S. M., Ash, D. E., Traish, A. M., and Christianson, D. W. (2001) Probing erectile function: *S*-(2-boronoethyl)-L-cysteine binds to arginase as a transition state analogue and enhances smooth muscle relaxation in human penile corpus cavernosum, *Biochemistry 40*, 2678−2688.
37. Cama, E., Colleluori, D. M., Emig, F. A., Shin, H., Kim, S. W., Kim, N. N., Traish, A. M., Ash, D. E., and Christianson, D. W. (2003) Human arginase II: crystal structure and physiological role in male and female sexual arousal, *Biochemistry 42*, 8445−8451.
38. Collet, S., Carreaux, F., Boucher, J.-L., Pethe, S., Lepoivre, M., Danion-Bougot, R., and Danion, D. (2000) Synthesis and evaluation of ω-borono-α-amino acids as active-site probes of arginase and nitric oxide synthases, *J. Chem. Soc., Perkin Trans. 1*, 177−182.

39. Cavalli, R. C., Burke, C. J., Kawamoto, S., Soprano, D. R., and Ash, D. E. (1994) Mutagenesis of rat liver arginase expressed in *Escherichia coli*: role of conserved histidines, *Biochemistry 33*, 10652−10657.
40. Otwinowski, Z., and Minor, W. (1997) Processing of X-ray diffraction data collected in oscillation mode, *Methods Enzymol. 276*, 307−326.
41. Navaza, J. (1994) *AMoRe*: an automated package for molecular replacement, *Acta Crystallogr. A50*, 157−163.
42. Collaborative Computational Project, No. 4 (1994) The *CCP*4 suite: programs for protein crystallography, *Acta Crystallogr. D50*, 760−763.
43. Brünger, A. T., Adams, P. D., Clore, G. M., DeLano, W. L., Gros, P., Grosse-Kunstleve, R. W., Jiang, J. S., Kuszewski, J., Nilges, M., Pannu, N. S., Read, R. J., Rice, L. M., Simonson, T., and Warren, G. L. (1998) Crystallography and NMR system: A new software suite for macromolecular structure determination, *Acta Crystallogr. D54*, 905−921.
44. Jones, T. A., Zou, J.-Y., Cowan, S. W., and Kjeldgaard, M. (1991) Improved methods for building protein models in electron density maps and the location of errors in these models, *Acta Crystallogr. A47*, 110−119.
45. Esnouf, R. M. (1997) An extensively modified version of MolScript that includes greatly enhanced coloring capabilities, *J. Mol. Graphics 15*, 132−134.
46. Merritt, E. A., and Bacon, D. J. (1997) Raster3D: Photorealistic molecular graphics, *Methods Enzymol. 277*, 505−524.
47. Berman, H. M., Westbrook, J., Feng, Z., Gilliland, G., Bhat, T. N., Weissig, H., Shindyalov, I. N., and Bourne, P. E. (2000) The Protein Data Bank, *Nucleic Acid Res. 28*, 235−242.
48. Kuhn, N. J., Talbot, J., and Ward, S. (1991) pH-sensitive control of arginase by Mn(II) ions at submicromolar concentrations, *Arch. Biochem. Biophys. 286*, 217−221.
49. Bewley, M. C., Jeffrey, P. D., Patchett, M. L., Kanyo, Z. F., and Baker, E. N. (1999) Crystal structures of *Bacillus caldovelox* arginase in complex with substrate and inhibitors reveal new insights into activation, inhibition, and catalysis in the arginase superfamily, *Structure 7*, 435−448.
50. Han, S., Moore, R. A., and Viola, R. E. (2002) Synthesis and evaluation of alternative substrates for arginase, *Bioorg. Chem. 30*, 81−94.
51. Kanyo, Z. (1996) *The structure of rat liver arginase*, Ph.D. Thesis, University of Pennsylvania, Philadelphia, PA.
52. Cama, E., Emig, F. A., Ash, D. E., and Christianson, D. W. (2003) Structural and functional importance of first-shell metal ligands in the binuclear manganese cluster of arginase I, *Biochemistry 42*, 7748−7758.
53. Vallee, B. L., and Williams, R. J. P. (1968) Metalloenzymes: The entatic nature of their active sites, *Proc. Natl. Acad. Sci. U.S.A. 59*, 498−505.

BI0491705